Available online at www.sciencedirect.com
ScienceDirect
Earth and Planetary Science Letters 269 (2008) 80–95
EPSL
www.elsevier.com/locate/epsl

A 53 year seasonally resolved oxygen and carbon isotope record from a modern Gibraltar speleothem: Reconstructed drip water and relationship to local precipitation

David Mattey [a,*], D. Lowry [a], J. Duffet [a], R. Fisher [a], E. Hodge [b], S. Frisia [c]

[a] Department of Earth Sciences, Royal Holloway, University of London, Egham, Surrey, TW20 0EX, UK
[b] ANSTO Institute for Environmental Research, Lucas Heights, PMB 1, Menai, NSW 2234, Australia
[c] School of Environmental and Life Sciences, University of Newcastle, University Drive, Callaghan NSW 2308, Australia

Received 29 September 2007; received in revised form 11 January 2008; accepted 31 January 2008
Available online 19 February 2008
Editor: H. Elderfield

Abstract

The response of a climate proxy against measured temperature, rainfall and atmospheric circulation patterns at sub-annual resolution is the ultimate test of proxy fidelity but very few data exist showing the level of correspondence between speleothem climate proxies and the instrumental climate record. Cave sites on the Gibraltar peninsula provide a unique opportunity to calibrate speleothem climate proxies with the longest known available precipitation isotopes and instrumental records. An actively growing speleothem sampled from New St. Michaels Cave in 2004 is composed of paired laminae consisting of light columnar calcite and a darker microsparitic calcite. Stable isotope analysis of samples micromilled in 100 μm steps at the equivalent of bi-monthly intervals reveals fabric-correlated annual cycles in carbon isotopes, oxygen isotopes and trace elements responding to seasonal changes in cave microclimate, hydrology and ventilation patterns. Calcite $\delta^{13}C$ values reach a minimum in the light columnar fabric and evidence from trace element behaviour and cave monitoring indicates that this grows under cave 'winter' conditions of highest pCO_2, whereas the dark microsparitic calcite, characterised by elevated $\delta^{13}C$ and $\delta^{18}O$ values grows under low 'summer' pCO_2 conditions. Drip water $\delta^{13}C_{DIC}$ reaches a minimum in March–April, at which time the attenuated $\delta^{18}O$ signal becomes most representative of winter precipitation. An age model based on cycle counting and the position of the ^{14}C bomb carbon spike yields a precisely dated winter oxygen isotope proxy of cave seepage water for comparison with the GNIP and instrumental climate record for Gibraltar. The $\delta^{18}O$ characteristics of calcite deposited from drip water representing winter precipitation for each year can be derived from the seasonally resolved record and allows reconstruction of the $\delta^{18}O$ drip water representing winter precipitation for each year from 1951–2004. These data show an encouraging level of correspondence ($r^2=0.47$) with the $\delta^{18}O$ of rainfall falling each year between October and March and on a decadal scale the $\delta^{18}O$ of reconstructed winter drip water mirrors secular change in mean winter temperatures.

Keywords: speleothem; Gibraltar; oxygen isotopes; GNIP; precipitation; seasonality

1. Introduction

Speleothem are calcium carbonate deposits which can be precisely dated and provide accurate records of climate change in the past (Henderson, 2006). Studies of oxygen and carbon isotope ratio records have led to significant advances in the understanding of temperature and continental precipitation variability in the last 400,000 years (McDermott, 2004; Fairchild et al., 2005). Nearly all speleothem isotope proxy studies have focussed on long-term change observed at the centennial-millennial scale (e.g. McDermott et al., 2001; Yuan et al., 2004) but the climate driven responses of oxygen isotope time series recorded in speleothem remain largely untested against modern

* Corresponding author.
E-mail address: mattey@gl.rhul.ac.uk (D. Mattey).

0012-821X/$ - see front matter © 2008 Elsevier B.V. All rights reserved.
doi:10.1016/j.epsl.2008.01.051

instrumental records. Several studies have tested the correspondence between the isotopic composition of precipitation and seepage waters over short periods (e.g. Ayalon et al., 1998; Mickler et al., 2004; Cruz et al., 2005) but opportunities for vital longer comparisons, which will provide a more holistic view of the effects of changing precipitation and temperature patterns, are very limited because long precipitation isotope records exist for relatively few localities (e.g. those available in the GNIP data base IAEA/WMO, 2004). Long instrumental climate records are far more widely available and Treble et al. (2005a) showed that a modern speleothem that grew between 1911 and 1992 in Moondyne Cave, SW Australia preserved seasonal cycles in $\delta^{18}O$ but the decadal trends in $\delta^{18}O$ and $\delta^{13}C$ were more difficult to reconcile with observed changes in temperature or precipitation. Observation of seasonality in the speleothem isotopic record (Treble et al., 2005a; Mattey et al., 2005; Johnson et al., 2006) highlights the importance of understanding causes of seasonal components in the speleothem isotopic signal and provides opportunities for vital comparisons with instrumental records at inter-annual resolution.

Validation of speleothem climate proxies ideally requires a set of criteria and conditions that are not always possible to meet. A cave site at or very near to a location where a long instrumental record has been kept is pre-requisite to avoid bias caused by potentially significant local differences in temperature and rainfall patterns. Active speleothem growth needs to be at a site within the cave which has microphysical conditions that are not conducive to adverse isotopic fractionation, with a rate of calcite growth fast enough to produce annual laminae that are thick enough for sampling at sub-annual resolution. Knowledge of the hydrological response of seepage water to seasonal rainfall patterns is needed to know timescales of water storage and mixing in the karst aquifer (Tooth and Fairchild, 2003). Finally, a precise age model is required to correlate the speleothem $\delta^{18}O$ time series with the climate record at the inter-annual scale.

Cave sites on the Gibraltar peninsula meet the requirements specified above and provide a unique opportunity to calibrate actively growing speleothem $\delta^{18}O$ with one of the longest available precipitation isotopes and instrumental climate records. Here we report fabric-correlated cycles in high resolution stable isotope and trace element time series, which, in conjunction with cave monitoring data, show that the cycles are unequivocally related to seasonal changes in cave microclimate and hydrology. The seasonally resolved time series provide an oxygen isotope proxy record of winter precipitation that is accurately tied to calendar years by counting cycles from the time of collection. The age model is confirmed by location of the atmospheric ^{14}C bomb carbon peak. These data provide a robust relationship between speleothem calcite fabrics, seepage waters and precipitation at seasonal resolution over a 50 year period and, to date, the longest possible inter-annual

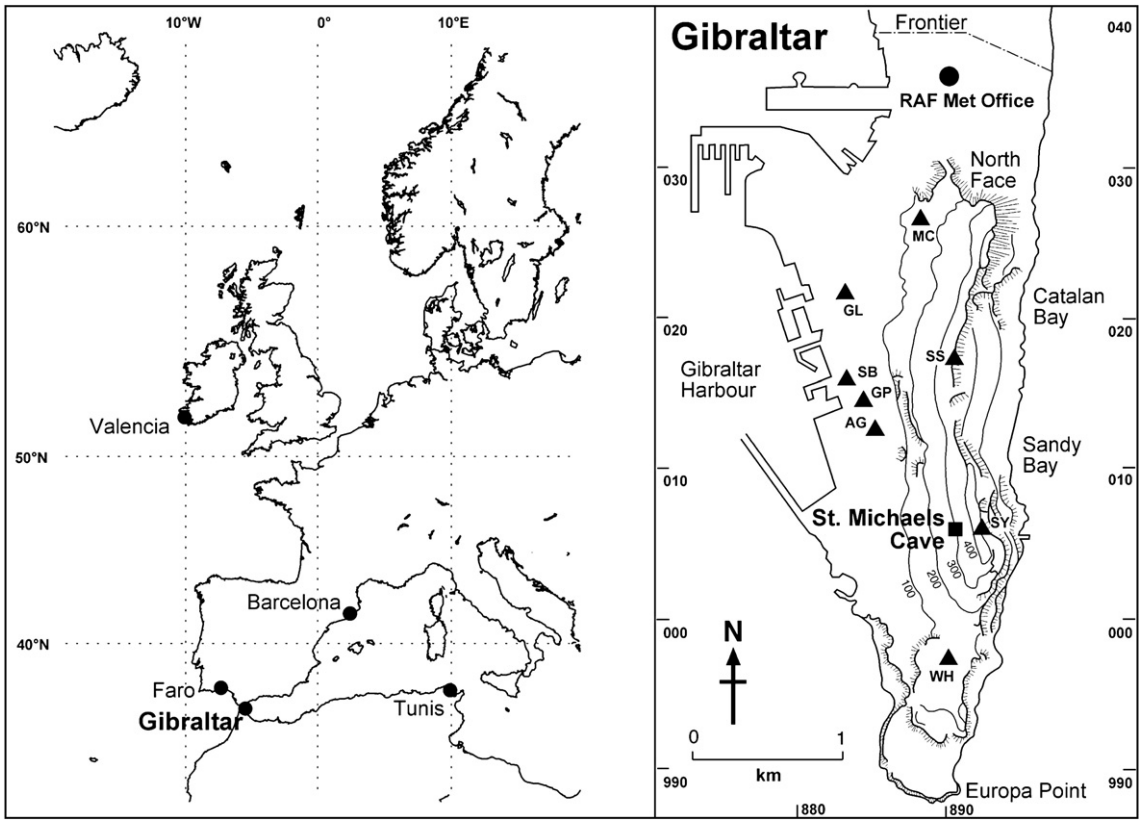

Fig. 1. Left: Location of Gibraltar and the maritime GNIP sites where more than 20 years of precipitation isotope data are available (IAEA/WMO, 2004). Right: Location map of St. Michaels Cave, the RAF Met Office and nearby historic weather station sites (triangles) with 1000 m UTM grid co-ordinates. Historic locations from Wheeler (2006); MC Moorish Castle, GL Garrison Library, SS Signal Station, SB South Bastion, GP Grand Parade, AG Alameda Gardens, SY Spyglass Battery, Windmill Hill.

comparison of the $\delta^{18}O$ of precipitation and $\delta^{18}O$ of speleothem calcite.

2. Sampling and analytical methods

2.1. Setting

The Gibraltar peninsula (36°9' N, 5°21' W) is a unique maritime location at the western entrance to the Alboran Basin, where airflows are channeled E–W between the Sierra Nevada in Spain and Atlas Mountains in N. Africa (Fig. 1). Weather data have been collected in Gibraltar since the late 18th century from various locations on the peninsula, initially from town locations near the South Bastion by the British garrison until 1929, then from Alameda botanical gardens and Windmill Flats until the establishment of the RAF Met Office station from 1947 (Fig. 1) (Wheeler, 2006). Together, these sources yield one of the longest instrumental climate records in the Mediterranean region with monthly rainfall amounts from 1792 (Wright et al., 1994), atmospheric pressure (and NAO index) from 1821 (Jones et al., 1997) and mean daily temperatures from 1822 (Wheeler, 2006). Furthermore, Gibraltar has been an IAEA precipitation sampling site since 1961 and there exists a monthly record of δD, $\delta^{18}O$ and tritium to the present day (IAEA/WMO, 2004).

The Gibraltar climate is semi-arid and strongly seasonal, with hot dry summers (1947–2004 average is 24.3 °C) and winters with a mixture of cool and wet periods (average 13.5 °C). The mean annual temperature (MAT) for the period 1947–2004 averages 18.3 °C. Decadal trends in MAT systematically decrease from 1947 reaching a minimum during 1970–5 (≈0.6 °C below average) then has risen to present day values which are now ≈0.5° above the 1947–2004 average. Annual rainfall from 1947 to 2004 averages 767 mm with >80% of precipitation occurring from October and March (see Table 1 in the Appendix) with multi-annual trends sensitive to the state of the North Atlantic Oscillation (NAO) (Xoplaki et al., 2004; Andreo et al., 2004; Andreo et al., 2006; Lopez-Bustins et al., in press).

Despite incomplete data for 1968 to 1971 and some other individual months the Gibraltar monthly precipitation isotope record (IAEA/WMO, 2004) is among the longest available in

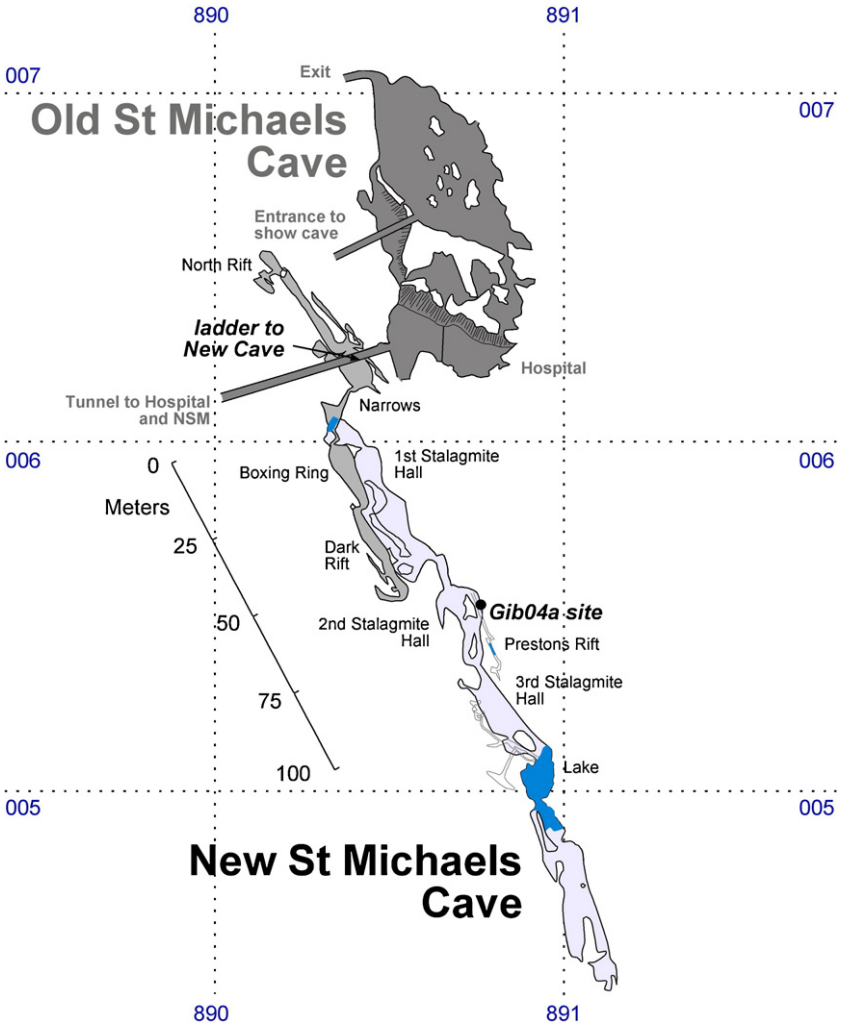

Fig. 2. Plan of the St. Michaels Cave system based on the original cave surveys (see Shaw, 1953a,b; Rose and Rosenbaum, 1991) positioned relative to 1000 m UTM grid co-ordinates after a new survey carried out in 2007. Location of the stalagmite sampling site Gib04a is shown.

Europe. Seasonality in precipitation $\delta^{18}O$ is evident in the monthly records with summer precipitation $\delta^{18}O$ typically about 2‰ higher than the mean winter (October–March) value (≈−4.5‰). Multivariate analysis of climate controls on precipitation $\delta^{18}O$ data binned at annual or monthly intervals reveal weak dependence on amount and temperature but individually sampled rain events show a significant ($r^2 \approx 0.6$) dependence on temperature (Mattey, unpublished data).

2.1.1. New St. Michaels Cave

A large number of natural karst cavities including the cave systems of St. Michaels (Shaw, 1953a,b) (Fig. 2) and Ragged Staff (Rose and Rosenbaum, 1991) open in the rock of Gibraltar, an isolated mass of limestone forming a 3 km long N–S trending ridge reaching an altitude of 426 m above sea level (a.s.l.). The eastern face of the rock forms vertical cliffs and the western slopes are covered with dense scrub (maquis) and fall at an average angle of 35° down to the town at sea level. The rock also features extensive systems of tunnels developed for military and civic purposes which intersect, and sometimes exploit natural caves (Rose and Rosenbaum, 1991). Solution caves are mostly developed along the strike of a band of dolomitised Gibraltar limestone which dips steeply to the west (Rose and Rosenbaum, 1991). Caves are at least Pleistocene in age (Rodrıguez-Vidal et al., 2004) and initially formed under phreatic conditions and subsequently underwent phases of uplift and draining (Tratman, 1971). Old St. Michaels Cave is at an altitude of 325 m a.s.l. (Shaw, 1953a). New St. Michaels Cave system was discovered in 1942 (Shaw, 1953b) when a new entrance tunnel to the lower part of the Old St. Michaels show cave (known as the Hospital) exposed a lower rift system. These lead to a lower series of large chambers which contain a small lake. Locally active speleothem growth is taking place in a wet area located 100 m into the main chamber, near Preston's Rift (Fig. 2), forming roof straws, stalagmite bosses and areas of new flowstone. The calcite currently being deposited at active drip sites in New St. Michaels Cave has a distinctive translucent amber appearance and an actively growing stalagmite boss located on a shelf near the upper entrance to Preston's Rift was selected for this study. The present study focuses on this modern amber calcite which contains laminae pairs that are thick enough for high resolution sampling by micromill.

2.2. Cave monitoring

Cave environmental monitoring has been carried out since October 2004 with continuous logging of temperature, humidity, drip rates and pCO_2 values and monthly sampling of air and water for geochemical analysis (Mattey et al., 2005; Mattey et al., 2006). Drip water was collected for analysis using a HDPE beaker fitted with a drip logger (www.driptych.com) to record discharge, and an outlet tube leading to a storage vessel. Monthly aggregates taken from the vessel were stored in 100 ml HDPE doubly sealed bottles. pH, conductivity and alkalinity were measured on site and bottles were shipped to the UK, analysed for DIC $\delta^{13}C$ upon receipt, then stored at 4 °C for subsequent analysis of $\delta^{18}O$ and trace elements.

2.3. Speleothem fabric characterisation, microsampling and trace element analysis

The sample Gib04a was sectioned for petrographic study and fabric imaging by SEM and electron backscatter diffraction (EBSD). The EBSD image was obtained using an HKL Channel5 EBSD system on the Philips XL30CP SEM, in the School of GeoSciences, University of Edinburgh. The sample was mapped for crystallographic orientation in series of 8 grids of 342 × 256 points with a step distance of 2.7 μm between each point. The 8 areas were subsequently tiled together to form the completed map of 717,162 analyses, covering and area of 3.69 × 1.38 mm. At each point a diffraction pattern was imaged and indexed as either calcite or aragonite to determine the phase present and the crystallographic orientation of the sample at that point.

Sampling by hand drilling and micromilling was carried out for XRD analysis, U–Th dating and isotope analysis. Reconnaissance stable isotope data were obtained initially by low resolution drilling and then by laser ablation at 300 μm resolution (Spötl and Mattey, 2006). Sampling at 300 μm resolution revealed evidence of unresolved seasonal variations and high resolution sampling was carried out by contiguous micromilling at 100 μm resolution which resolved smooth cycles in $\delta^{13}C$ out of the strongly aliased data obtained by hand drilling and laser ablation (partially and fully resolved data are compared in Fairchild et al., 2005, Figure 12). Samples for the high resolution $\delta^{13}C$ and $\delta^{18}O$ time series were obtained by contiguous micromilling along a 3 mm wide trench cut parallel to laminae in 100 μm increments along the growth axis of the specimen. Trace element data were measured by *in-situ* UV laser ablation (266 nm) -ICPMS at 40 μm resolution using the NERC facility at the University of Kingston and are reported as count ratios relative to Ca, corrected for ionisation efficiency.

2.4. Isotope analysis

All isotopic analyses in this study were carried out using GV Instruments Multiflow-Isoprime systems at Royal Holloway. Water samples were aliquots of monthly collections and analysed for $\delta^{13}C$ DIC by acidification of 0.5 ml of water with orthophosphoric acid and equilibrating for 4 h at 40 °C. $\delta^{13}C$ values were normalised to the V-PDB scale via a calibrated sodium bicarbonate internal standard and have an external reproducibility of better than 0.08‰. Water $\delta^{18}O$ was analysed as a rolling program of reanalysis of the previous three months of sampling with each new set of samples to provide the highest level of consistency along the time series over the monitoring period. Each sample was analysed in duplicate during at least 4 different sessions by equilibration of 0.2 ml water with 5% CO_2–95% He for 7 h at 40 °C providing a long-term external reproducibility usually better than ±0.05‰. $\delta^{18}O$ values were normalized to V-SMOW using an internal standard DEW-1 (−8.45‰) calibrated to V-SMOW and V-SLAP.

Stable isotope analysis of carbonates was performed on 200 μg of powder by digestion in 105% orthophosphoric acid at 90 °C using a GV Instruments Multiflow He-flow system. $\delta^{13}C$

and $\delta^{18}O$ were measured on 9 consecutive injections of CO_2 giving an external precision of better than ±0.10‰ and data normalised to the PDB scale using data obtained for NBS-19 and house standards measured every 11 samples.

2.5. Radiocarbon analyses

In order to locate the position of the 1960s atmospheric radiocarbon (^{14}C) bomb-spike to use as a chronostratigraphic marker, ~5 mg samples were micromilled along 500 μm wide bands following laminae and carefully mapped to the central axis of the micromill traverse used for the $\delta^{13}C$ and $\delta^{18}O$ time series. Samples were converted to graphite using conventional techniques (Hua et al., 2001) and measured on the 2 MV HVEE "STAR" accelerator in the Institute for Environmental Research, ANSTO (Fink et al., 2004).

3. Results and discussion

3.1. Macroscopic features, petrography and mineralogy of Gib04a

3.1.1. Macroscopic features

The sample Gib04a was collected in June 2004 and consisted of three low bosses covered with amber calcite that drapes over surrounding flowstone and broken roof straws. The sample studied was 110 mm high and 50–60 mm wide, and has the thickest accumulation of young calcite. The internal structure is shown in Fig. 3 and is divided into an upper edifice of paler translucent microporous amber calcite and a lower edifice of darker compact amber calcite showing well developed light bands. The upper edifice is 45 mm thick and consists of pairs of dark and light laminae which average 750 μm and in places reach up to 1.5 mm in thickness. The light laminae in these couplets are laterally more variable in thickness, but tend to become the dominant fabric where the calcite begins to drape down the sides of the stalagmite.

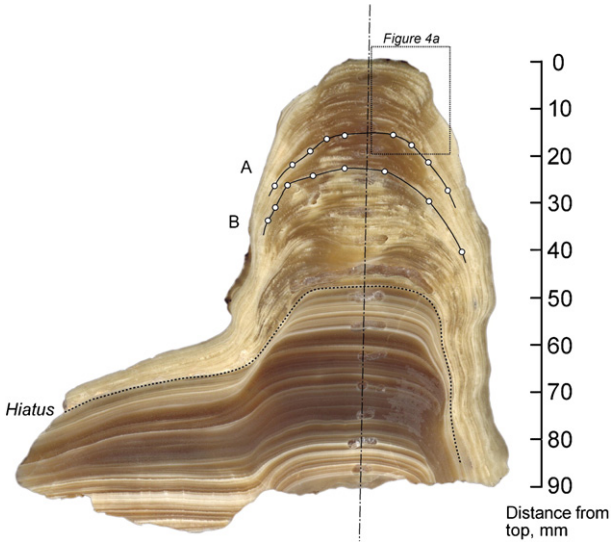

Fig. 3. Cut section of Gib04a showing macroscopic features and sampling locations for dating and Hendy tests A and B. The dotted line marks the position of the junction between the faster growing upper edifice and the lower edifice, where laminae are generally thinner and lithologies are laterally more persistent. The location of section illustrated in Fig. 4a is also shown.

A very thin layer of dark detritus, only visible in thin section, marks the change to the underlying, more compact edifice (Fig. 3). The structure of the laminae structure remains similar but differs from that in the overlying, more porous stalagmite portion because laminae are thinner and extend laterally without changing thickness or porosity. The bulk of this speleothem calcite is dark brown containing fine laminae defined by slight colour change on a scale of around 200 μm. Groups of pale thin bands are concentrated just below the junction and again at bottom of the section and these tend to be laterally more continuous than the pale bands present in the younger edifice.

3.1.2. Petrography and mineralogy

Macroscopic, thin section, scanning electron microscope and electron backscatter diffraction images illustrating features of the couplets in young, microporous calcite are shown in Fig. 4. Despite the presence of elongated crystals arranged in fan-like structures similar to those observed in aragonite speleothems, the mineralogy of the specimen was confirmed to be entirely calcite by using a number of techniques, including a synchrotron-based micro XRD map performed at ID22 of the European Synchrotron Radiation Facility (ESRF). Conventional XRD scans were performed on powders microdrilled from individual dark and light laminae both in the younger and older portions of the speleothem and all scans show only calcite diffraction peaks. EBSD mapping of a 3.7×1.4 mm region on the same slice (Fig. 4g) in 2.7 μm steps gave solutions that were consistent with a calcite mineralogy.

The light and dark laminae visible in hand specimen (Fig. 4a) are related to changes in the calcite fabric. In plane polarised light (Fig. 4b) the light calcite portion of the lamina is characterised by the presence of inter-crystalline macropores, elongated in the same direction as the growth axis of the stalagmite. The dark calcite portion is microsparitic and compact. Scanning electron microscope (SEM) images of fractured surfaces are shown in Fig. 4d–f. The light bands are composed of columnar calcite crystals 120 to 150 μm wide and up to 1.5 mm long with scattered macropores developed parallel to grain boundaries (Fig. 4d and e). The gradation from light to dark bands seen on polished surfaces is marked by loss of macropores and greater microporosity in the darker microsparitic fabric (Fig. 4e and f). A grain boundary map generated by electron backscatter diffraction (Fig. 4g) reveals the gross cyclical changes in calcite grain elongation defining the light and dark couplets and irregular laminae surfaces. The EBSD study shows that the c-axes of calcite forming both columnar and microsparite fabrics are closely aligned and, in this image, are oriented at an angle of 15° to the thin section (Mattey, unpublished data) so the true extent of grain elongation appears slightly foreshortened in Fig. 4g. Fabric development will be discussed in more detail elsewhere but the irregular boundaries between columnar and microsparitic fabrics seen in Fig. 4g have implications for sub-millimetre sampling whereby micromill

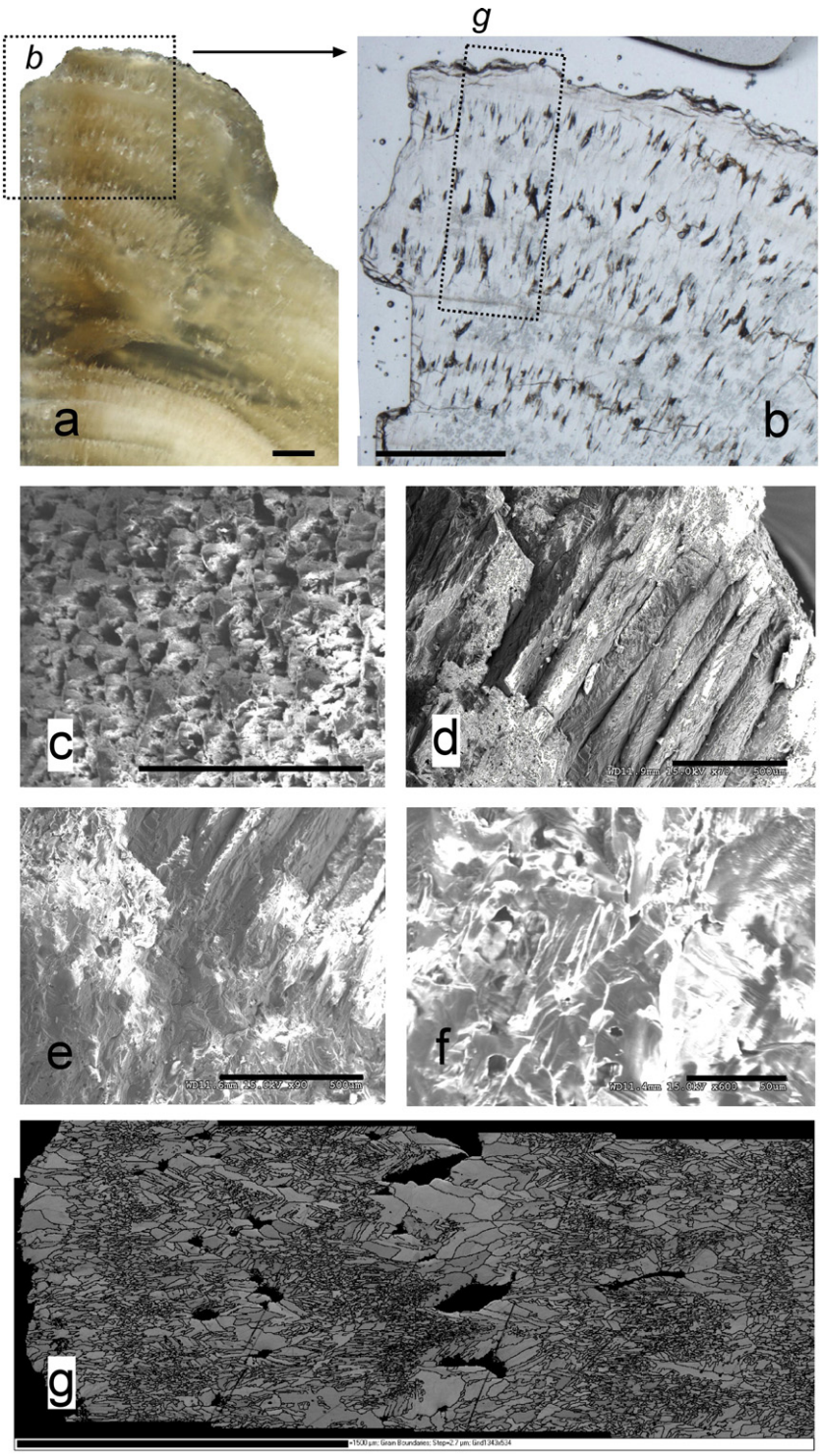

Fig. 4. Petrographic and crystal morphological features of dark compact (DC) and light columnar calcite (LCC) couplets from the upper portion of Gib04a. a) Polished section of a slice from area identified in Fig. 3. The active growth surface is uppermost. Scale bar = 1 mm. The faint vertical dark band is synchrotron radiation damage and marks the traverse followed to obtain the Sr profile plotted in Fig. 7. b) Thin section of slice cut parallel to surface shown in (a) viewed in plane polarised light. Scale bar = 1 mm. Dotted area shows region studied using electron backscatter diffraction in figure 4g. c) Scanning electron microscope (SEM) image of active growth surface showing LCC calcite columns with rhombohedral terminations. Scale bar = 1 mm. d) SEM image of fractured surface showing columnar crystals forming the LCC laminae. Columnar calcite is seen in image b as bands with vertical lines defining grain boundaries. Scale bar = 500 μm. e) SEM image of fractured surface showing boundary between LCC (upper right) and dark microsparitic calcite (DC, lower left). Scale bar = 500 μm. f) SEM image of fractured surface of microsparitic DC showing irregular intergranular porosity. Scale bar = 50 μm. g) Grain boundary map obtained by electron backscatter diffraction of area identified in (b). The LCC and DC fabrics are clearly defined and have very similar *c*-axis orientations. Width of image = 3.7 mm. See text for discussion.

traverses cut parallel to laminae may sample variable mixtures of each fabric.

3.1.3. Laminae couplets

The dark-light paired laminae present in the younger speleothem resemble the couplets described in Belgian speleothem by Genty and Quinif (1996) as being composed of alternating bands of 'white porous' and 'dark compact' palisade calcite. These couplets were interpreted as annual cycles that formed in response to changing water excess, with the dark compact layers deposited under wetter winter conditions. In the Gibraltar speleothem the light columnar calcite shows elongated macropores, but a well developed microporosity also characterizes the dark, more compact microsparite fabric. For the purposes of this study we adopt the terms 'dark calcite' (DC) and 'light columnar calcite' (LCC) to describe the macroscopic appearance of couplets seen in hand specimen and on polished slabs. DC corresponds to 'microsparite calcite' and LCC to 'columnar calcite' as defined by Frisia et al. (2000) and this study shows that these couplets are intimately correlated with geochemical cycles in trace elements and stable isotopes.

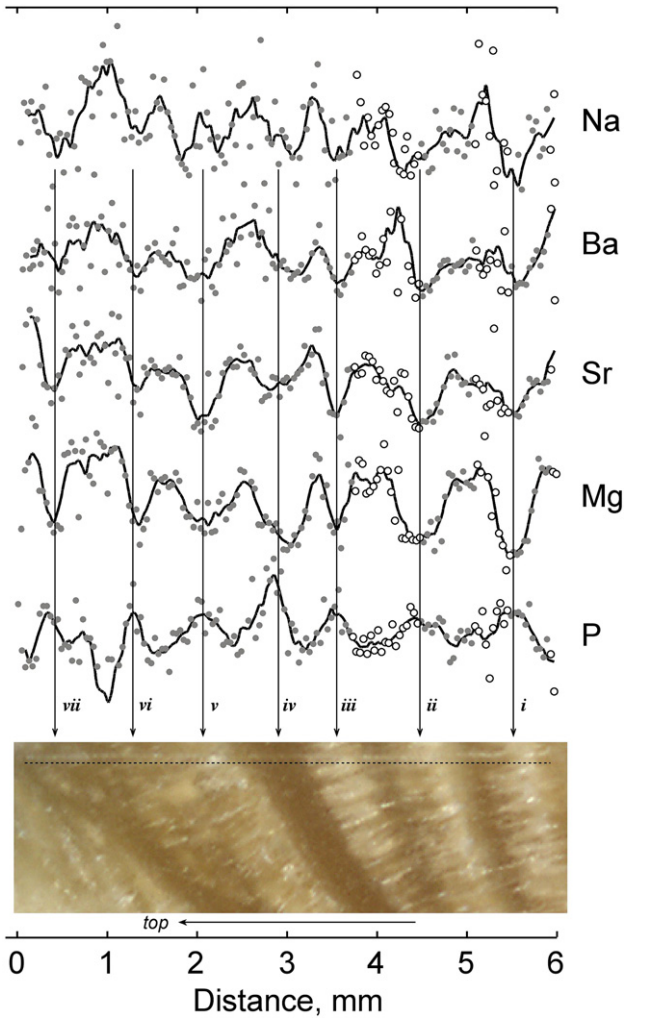

Fig. 5. Variation of Na, Ba, Sr, Mg and P measured by UV laser ablation-ICP-MS at 60 μm resolution along a 6 mm traverse across alternate LCC and DC fabrics. Line of traverse is visible just below top edge of image, above dotted reference line and younging direction is to the left. Data are scaled as nominal count ratios relative to Ca and fitted curves are 10 point moving averages. Open symbols are spots positively identified as LCC fabric at the time of analysis.

3.2. Trace element cycles

Annually resolved trace element patterns in speleothem are indicative of the hydrochemical regime and timing of seasonal growth and provide links between the hydrological cycles and fabric development relative to the calendar year (Huang and Fairchild, 2001; Fairchild et al., 2001; Treble et al., 2002; McMillan et al., 2005). Trace element patterns along a representative 6 mm traverse across paired laminae measured at 60 μm resolution by LA-ICMS are shown in Fig. 5. These data clearly show seven well developed cycles (numbered *i* to *vii*) in Mg, Sr, Ba and P. In common with some other studies of trace element variations in speleothem laminae (e.g. Fairchild et al., 2001; Treble et al., 2002), P shows an antipathetic relationship with the covarying Mg, Sr (and Ba) cycles. Trace element variability is broadly correlated with fabric, with P peaking, with the exception of cycle iv, in the white porous lamina. Na does not show clear cycles, although it broadly follows the trends shown by Mg, Sr and Ba.

The relationship between trace elements and fabric in Fig. 5 are slightly ambiguous as paired LCC and DC fabrics are only clearly developed on the right hand part of the traverse (cycles *i–iii*). The fabric relationships through cycles *iv* to *vii* become less distinct. The line of the ablation traverse is visible near the top edge of the image in Fig. 5 and when it was possible to positively identify the fabric through the optical viewing system during the analytical run, spots analysed in LCC are highlighted as open circles. The data for cycles *i–iii* and cycle *v* clearly show that maxima in P and minima in Mg, Sr and Ba occur within the LCC bands. DC bands are characterised by falling P and steeply rising Mg, Sr and Ba. The minimum value of P and maximum values of Mg, Sr and Ba are located close to the transition from DC back to LCC. The cyclicity remains persistent in the left half of the traverse but the correspondence between trace elements and fabric is less distinct through cycles *iv–vii*. Close inspection suggests a similar relationship where minima in P are located in slightly darker regions (=poorly defined DC bands). The exception to this is cycle *iv* where a strong maximum in P (accompanied by a weak minimum in Sr) occurs in the middle of a wide DC band.

These observations suggest that paired fabrics may not always fully develop as the system passes through each hydrochemical cycle but where couplets are clearly formed the relationships can be summarised as follows: the transition from DC to LCC is marked by falling Mg, Sr and Ba and rising P; the maximum in P (and minimum Mg etc) is located near the middle of the LCC fabric. As the remaining LCC continues to grow, P falls and Mg rises and the DC fabric returns just before peak levels of Mg, Sr and Ba are reached. New trace element time series have been obtained by synchrotron radiation micro-XRF and a longer profile for Sr is illustrated in Fig. 7 which shows the persistent and regular nature of the hydrochemical cycles.

Trace element behaviour provides clues as to the timing of the growth of the LCC and DC fabrics relative to hydrochemical cycles. Mg and Sr abundances in drip water are inherited from dissolution of dolomitised bedrock and enriched by prior calcite deposition elsewhere in the karstic groundwater system (Fairchild et al., 2000). Drip water Mg/Ca and Sr/Ca show strong seasonal variation (Mg/Ca shown in Fig. 7) and are highest in the late summer when discharge rates and cave air pCO_2 are lowest and, consequently, supersaturation is higher. Highest Mg and Sr concentrations are located in the DC which indicates this calcite was deposited in late summer from fluids which were more supersaturated that the winter's water. Experimental studies indicate that Sr incorporation in calcite may increase as supersaturation rises (Wasylenki et al., 2005). In contrast, the P-enriched, Mg and Sr depleted LCC fabric was deposited when water flow was higher and/or cave pCO_2 was highest, and supersaturation lower, in winter. Phosphorus is an indicator of bioactivity in the soil and the elevated levels of within the WCC fabric mark the onset of the winter flush when P is flushed from soil by the first winter rains (Huang and Fairchild, 2001).

3.3. A seasonally resolved $\delta^{13}C$ and $\delta^{18}O$ time series

Carbon and oxygen isotope values measured on the micromilled powders are shown in Fig. 6. The temporal resolution of the isotope time series is typically bi-monthly, and near-monthly where lamina thickness exceeds 1 mm. The carbon isotope data clearly reveal regular oscillations about a relatively constant mean value of −11‰. The lowest $\delta^{13}C$ values are typically around −12‰ and rise by 1–2‰ before falling back to this base value. This pattern is intimately related to the fabric of the paired laminae where the lowest $\delta^{13}C$ values are located in LCC and then $\delta^{13}C$ rises as the DC fabric develops, reaching a maximum just before the onset of the next layer of LCC. The accompanying $\delta^{18}O$ profile is more complex but also shows oscillations that partially follow the seasonal excursions in $\delta^{13}C$ (see discussion below) but the $\delta^{18}O$ cycles are small (<1‰), more irregular and superimposed on longer-term trends showing shifts of up to 2‰ (Fig. 6).

The regular and persistent cyclicity in $\delta^{13}C$ is strong evidence for seasonal control of the calcite precipitation process and the development of paired speleothem fabrics (Genty and Quinif, 1996). The seasonal effects of changing hydrology have been identified in high resolution studies of trace element patterns (Roberts et al., 1988; Finch et al., 2001; Huang and Fairchild, 2001; Fairchild et al., 2001; Treble et al., 2002) but clearly resolved annual variation in $\delta^{18}O$ and $\delta^{13}C$ attributable to seasonal effects have so far been more elusive and only recently demonstrated by ion probe (Treble et al., 2005a) and micromilling (Johnson et al., 2006).

3.3.1. Hendy tests and local isotopic disequilibrium processes

The partial seasonal coupling of calcite $\delta^{13}C$ and $\delta^{18}O$ in Fig. 6 may be a result of one or a combination of local and environmental processes. Local processes creating kinetic fractionation and correlated $\delta^{13}C$ and $\delta^{18}O$ patterns include seasonal changes in cave microclimate (e.g. changing humidity) or variable kinetic fractionation associated with large changes in the rate of CO_2 degassing (driven by variable drip rate or changing cave air pCO_2). Alternatively, variations in calcite $\delta^{13}C$ and $\delta^{18}O$ may be driven by different environmental processes that operate in the same sense over part of the seasonal cycle.

The striking pattern of $\delta^{13}C$ variation in Fig. 6 resembles seasonal changes in $\delta^{13}C$ of drip water bicarbonate observed elsewhere (Bar-Matthews et al., 1996; Baker and Genty, 1998; Spotl et al., 2005) where drip water bicarbonate $\delta^{13}C$ becomes elevated with respect to the $\delta^{13}C$ values of water formed in contact with CO_2 evolved from soil, as a result of CO_2 degassing under lower pCO_2 environments. Drip water $\delta^{18}O$

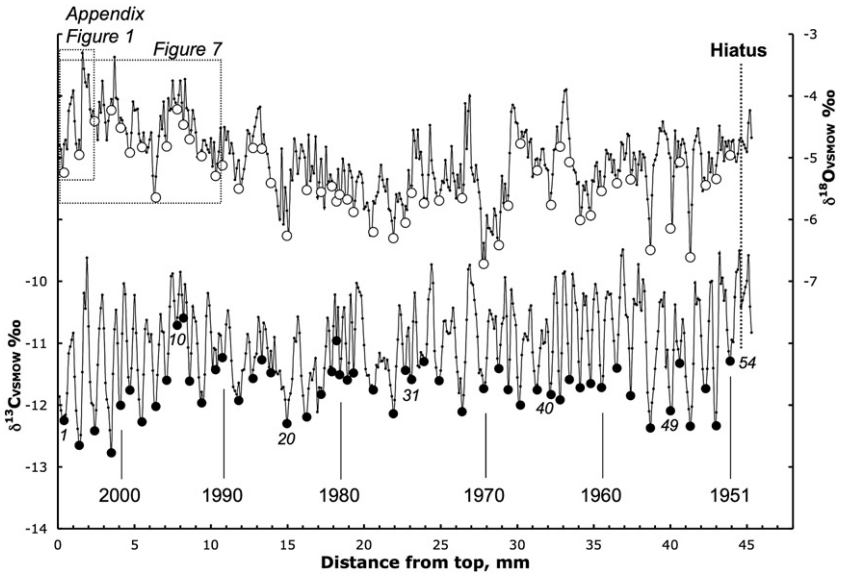

Fig. 6. The $\delta^{13}C$ and $\delta^{18}O$ time series obtained by contiguous micromilling in 100 μm steps plotted as a function of distance from top of Gib04a. $\delta^{13}C$ minima representing calcite deposition in April are marked with closed circles and the corresponding $\delta^{18}O$ value is plotted as open circles. Cycle numbers (italics) and age model relative to year 2004 are also shown (see text for explanation of age model).

could be responding simultaneously to the seasonal shifts in incoming drip water (derived from isotopically light winter rain and heavier summer rain, amplified by evaporation from the unsaturated zone during the summer drought) but covariance between $\delta^{13}C$ and $\delta^{18}O$ is also strongly linked to the issue of whether the calcite precipitation process is associated with variable degrees of kinetic fractionation (e.g. Mickler et al., 2004). Results of 'Hendy' tests (Hendy, 1971) are reported in the supplementary data in the Appendix and do not reveal any strong evidence of symmetrical trends in $\delta^{13}C$ or $\delta^{18}O$ that are consistent with kinetic effects but this is a problem that is difficult to resolve conclusively without carrying out *in-situ* deposition experiments where the spatial isotopic effects of calcite deposition can be measured directly. However in Gibraltar it is probably that kinetics are driven by physical processes in the cave that are ultimately related to climate.

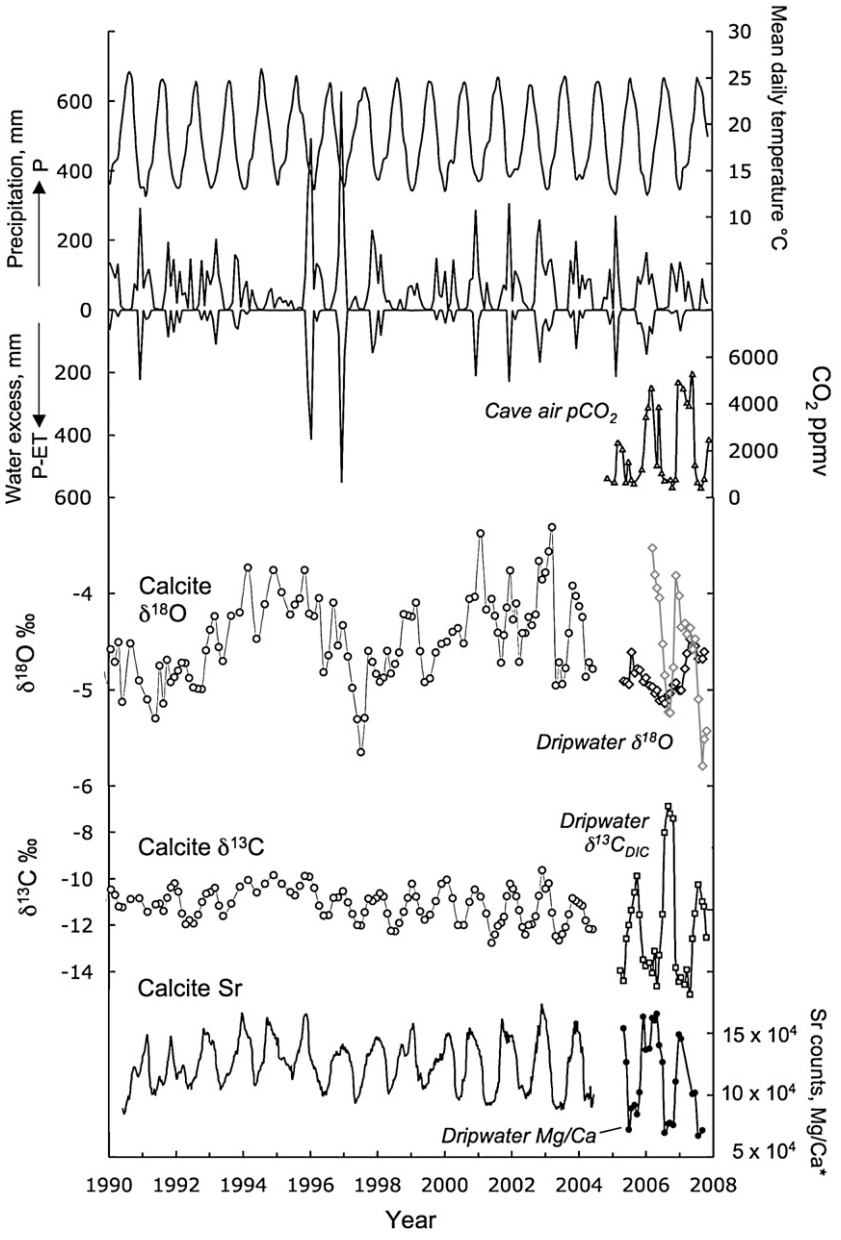

Fig. 7. Seasonality in Gibraltar climate compared to variations in cave air, Gib04a drip water and speleothem isotope and trace element cycles for the period 1990–2007. The upper part of the figure illustrates the highly seasonal Gibraltar climate over an 18 year period with curves for mean daily temperature, daily precipitation and monthly water excess (P-ET, calculated using the Thornthwaite method Thornthwaite, 1954). The pCO_2 in cave air measured at monthly intervals since 2004 from the Gib04a site is plotted as closed triangles. The lower part of the figure shows annual variations in the $\delta^{18}O$, $\delta^{13}C$ and Sr composition of speleothem calcite from 1990 to 2004 (based on the age model discussed in the text), and in drip water $\delta^{18}O$, $\delta^{13}C$ and Mg/Ca sampled at monthly intervals from 2004 to 2007. Drip water $\delta^{18}O$: diamonds — Gib04a site; grey diamonds — Dark Rift. Calcite Sr data are Sr kα counts measured in 10 μm steps by synchrotron micro-XRF at ID22, European Synchrotron Radiation Facility. Drip water Mg/Ca is expressed as 10^5 * Mg/Ca to plot on same scale as Sr data. Note that winter low temperatures and peak recharge correspond to high cave air pCO_2 levels, low drip water $\delta^{13}C$ values, and high drip water Mg/Ca ratios. Meteorological data adapted from Crown copyright data supplied by the Met Office.

3.4. Cave monitoring evidence for seasonality in cave microclimate and drip water chemistry

Monthly cave monitoring of soil and cave air, cave hydrology and drip water chemistry has been ongoing since summer 2004 (Mattey et al., 2005; Mattey et al., 2006) and provides vital insight on the cause of annual $\delta^{13}C$ fluctuations and the evolution of drip water $\delta^{18}O$. Some of the more important results of the ongoing monitoring are summarised below. The monitoring sites are situated about 100 m from the show cave area and separated from them by constricted passages (Fig. 2). Temperature at the Gib04a site, 17.9±0.2 °C, and humidity, >95%, buffered by the nearby lake, do not show detectable seasonal variation and changes in evaporation rate are not believed to be the underlying cause of seasonal shifts in $\delta^{13}C$ and $\delta^{18}O$. The roof thickness above the GibO4a site is 60 m and the Gib04a seepage discharge rates respond approximately 2 weeks after the onset of the first winter rain. The Gib04 discharge variance is low and show gradual seasonal changes from 0.1 µl/s during summer 2005 to a peak of 0.6 µl/s in winter 2005/6 before returning to a new minimum of 0.3 µl/s in summer 2006. No surges responding to discrete rain events were recorded. Drip water pH, Ca and Mg/Ca appear to be correlated with discharge rate with clear evidence of greater calcite saturation and more extensive calcite precipitation during the low summer discharge period.

Some of the results of cave monitoring are summarised in Fig. 7 and compared with 18 years of temperature, precipitation and aquifer recharge (P-ET) records from Gibraltar. Also plotted are the last 15 cycles in Sr, $\delta^{13}C$ and $\delta^{18}O$ in Gib04a scaled to calendar years, based on an age model described below. Soil air and cave air spot sampling shows that pCO_2 in the soil is related to temperature and moisture availability (Miotke, 1974; Amundson and Davidson, 1990) and peaks in May–June then rapidly declines as the summer drought develops. Measurements of pCO_2 in cave air (e.g. Baker and Genty, 1998; Bourges et al., 2001; Spotl et al., 2005; Faimon et al., 2006; Batiot-Guilhe et al., 2007) commonly (but not always Hoyos et al., 1998) show that cave air pCO_2 is highest during the summer, but in Gibraltar cave air pCO_2 (shown in Fig. 7) rises sharply in mid-November reaching winter values of 5000 ppmv, and then falls sharply to less than 1000 ppmv in mid-April, well before the water availability *and* soil CO_2 supply starts to decline during the summer drought. The controls on cave air pCO_2 are complex and recent data obtained by continuous multichannel logging reveal that the winter rise in cave air pCO_2 is primarily a result of reversals in chimney ventilation driven by temperature contrast between the cave interior and the outside, with additional transient effects caused by synoptic scale atmospheric pressure and wind conditions.

Drip water pH, alkalinity, Ca, Mg and Sr abundances and the $\delta^{13}C$ of dissolved bicarbonate all track the seasonal rise and fall in cave air pCO_2 which is controlling degassing and calcite supersaturation. The lowest value of drip water $\delta^{13}C$ and highest Mg/Ca values occur at the end of winter when the cave switches to summer mode and highest $\delta^{13}C$ values and greatest degrees of calcite supersaturation develop in September (Fig. 7). As previously mentioned, it is likely that Sr incorporation in calcite is also favoured by higher calcite supersaturation (Wasylenki et al., 2005). The antipathetic relationship between $\delta^{13}C$ and Mg/Ca or Sr (c.f McDermott et al., 2006; Fairchild and McMillan, 2007) is another indicator of seasonally controlled cave microphysics in Gibraltar which promotes climate related kinetic effects through rapid degassing when there is lowest cave air pCO_2 in the summer.

The seasonal evolution of $\delta^{18}O$ in drip waters is shown in Fig. 7. All drip sites show attenuation of $\delta^{18}O$ relative to the annual range in precipitation as a result of storage and mixing (Yonge et al., 1985; Cruz et al., 2005) but each site still preserves significant seasonal variation ranging from 0.6‰ at the Gib04a site (a seepage flow drip with ≈2 week response to rain events, Fig. 7) to nearly 2‰ in the Dark Rift (a fracture flow drip with ≈6 h response to rain events). These observations show that a component of the calcite seasonal $\delta^{18}O$ signal, which is typically not more than 1‰ trough to peak (Figs. 6 and 7), must be related to seasonal isotopic evolution of stored water, possibly as a result of input of isotopically heavy summer rain or, more likely in a semi-arid climate, evapotranspiration from the unsaturated zone (Ayalon et al., 1998). Variable kinetic fractionation, forced by the cave microclimate in "summer" mode, might also contribute to the elevated $\delta^{18}O$ in summer calcite and the intra-annual correlation between $\delta^{13}C$ and $\delta^{18}O$ seen on Figs. 6–8, but this process remains unquantified.

3.5. Seasonal controls on the $\delta^{13}C$ and $\delta^{18}O$ of speleothem calcite and associated fabrics

3.5.1. The $\delta^{13}C$ seasonal cycle

A working hypothesis explaining annual $\delta^{13}C$ cycles and associated paired fabrics is based on seasonality in cave ventilation as the dominant forcing mechanism controlling calcite growth. In 'winter mode' (mid-November to mid-April) upward chimney-effect ventilation maintains high levels of cave air pCO_2 so calcite supersaturation is lower and intracrystalline pores remain open and filled with water. The 'winter' layer of calcite growing on to the stalagmite is composed of porous LCC (Frisia et al., 2000) with baseline $\delta^{13}C$ values around −12‰.

In 'summer mode' (mid-April–mid-November) the sharp fall in cave air pCO_2, caused by inward flow of ambient atmosphere, forces more rapid degassing and higher calcite supersaturation. Rapid precipitation of crystals, whose morphology is dictated by the various effects exerted by trace elements such as Sr and Mg, leads to growth of a 'summer' layer as compact DC fabric characterised by rising $\delta^{13}C$. These conditions also favour prior calcite precipitation as roof straws and elsewhere in the aquifer system (Tooth and Fairchild, 2003) which explains rising Mg/Ca values which reach a maximum in late summer. The onset of autumn rainfall and the switch to 'winter mode' ventilation in mid-November when pCO_2 rises decreases calcite supersaturation, Mg/Ca, Sr/Ca and results in a return to the LCC fabric as drip water $\delta^{13}C$ returns to its baseline value.

3.5.2. The $\delta^{18}O$ seasonal cycle

The monitoring data obtained so far suggest that a component of $\delta^{18}O$ cyclicity in the speleothem calcite may be

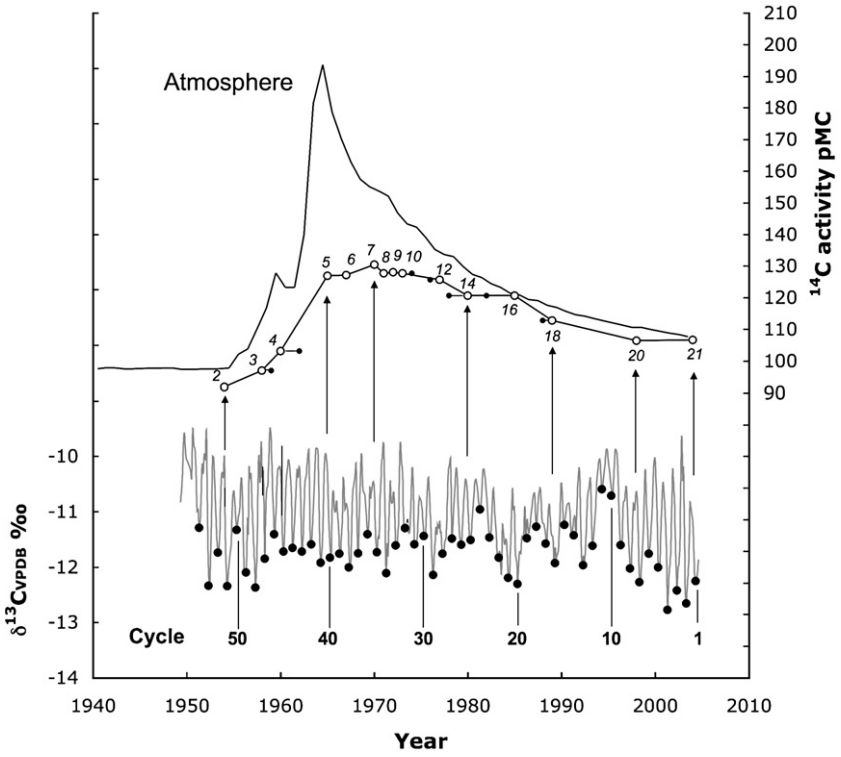

Fig. 8. ^{14}C activities (open circles) for individual laminae (labelled 2 to 21) plotted as a function of age determined by counting δ^{13}C minima (closed circles) back from the time of collection in 2004. The atmospheric ^{14}C bomb-pulse (Stuiver et al., 1998; Hua and Barbetti, 2004) is shown for comparison. Closed circles linked to ^{14}C values show locations where small differences exist between ^{14}C model ages and the δ^{13}C timescale (see text for discussion).

related to the hydrological cycle whose timescale depends on the timing and amount of recharge and the storage-flow characteristics of the aquifer. Relatively large seasonal changes in drip water δ^{18}O are a common feature of semi-arid climates (Yonge et al., 1985; Bar-Matthews et al., 1996), either as a result of evaporation of groundwater in the soil and epikarst or temperature control on the isotopic composition of precipitation which in Gibraltar may be up to 8‰ heavier than winter rain (Mattey, unpublished data). In addition the magnitude of a kinetic component may increase under 'summer' cave conditions when calcite supersaturation and reaction rates increase as a response to low cave pCO_2. Drip water with *lowest* δ^{18}O which arrives at the Gib04a site in early summer is the best proxy representing the isotopic composition of the recent winter rain. In this model the δ^{18}O of this 'winter' drip water provides an upper limit on the isotopic composition of winter precipitation which is attenuated by storage and mixing, but is most removed from the adverse processes that tend to operate during the 'climatic summer' (groundwater evaporation) or the 'cave summer', when higher calcite supersaturation and rapid precipitation rates may be conducive to greater kinetic effects.

3.5.3. Are the speleothem isotope cycles annual?

A key issue is whether the trace element, δ^{13}C and δ^{18}O cycles are annual and encode reproducible seasonal signals that can be correlated with the instrumental record. An annual component in the speleothem signal might be expected since the Gibraltar climate itself is highly seasonal. The monthly temperature, precipitation and water excess from 1990 to 2007 is illustrated in Fig. 7. 80% of annual rain falls between October and March but recharge is highly focused and peaks in December/January. The amount of recharge may vary considerably from year to year supporting the idea that evaporative loss from the soil zone may be an important factor in groundwater hydrochemistry. Temperature is also strongly seasonal and monitoring shows that temperature plays a key role in controlling cave air pCO_2 as a result of changing ventilation modes in winter and summer. The annual cycles observed in cave air pCO_2 and drip water chemistry provides compelling evidence that the speleothem δ^{13}C and trace element cycles in are annual features and form the basis of a reliable age model.

3.6. Age model based on counting of annual cycles and location of the atmospheric ^{14}C bomb-pulse

The anchor point for an age model for Gib04a is June 2004 when the actively dripping sample was collected. The active growth surface of Gib04a is shown in Fig. 4c and shows development of large rhombohedrally terminated crystal tips which correspond to the growth of light columnar calcite at the time of sampling. A high resolution micromill traverse in 50 μm steps across the tip of the sample (Mattey, unpublished data) shows that the very youngest calcite shows rising δ^{13}C values reaching −11.5‰, significantly higher than the δ^{13}C winter minimum of the previous year. These observations are consistent with a June 2004 date for the start of the time series. U–Th dating confirmed the age of the amber calcite above the junction as less than 300 years old but uncertainties resulting

from significant initial Th contributions limits the use of these dates in the age model.

The best evidence of annularity is provided by the very regular annual oscillations in $\delta^{13}C$ shown in Fig. 6, which yields a precise means of dating whereby the $\delta^{13}C$ minima mark conditions conducive to late winter growth under high cave pCO_2. The $\delta^{13}C$ minimae marked on Fig. 6 were identified using an algorithm that recognised 54 minima in the time series as far as the hiatus. The first and youngest minimum is taken to be April 2004 and the remaining 53 minima then defines 1951 as the age of the first annual cycle after the hiatus. The hiatus marks renewed growth probably as a result of documented exploration activities at this time (Shaw, 1953b) causing damage to hollow roof stalactites and rejuvenated water flow.

3.6.1. Bomb-pulse chronology

The ^{14}C activity in 15 individual laminae are presented in Table 1 in the Appendix, and their spatial positions mapped to $\delta^{13}C$ cycle numbers and model age are compared to the atmospheric bomb-pulse for the Northern Hemisphere (Stuiver

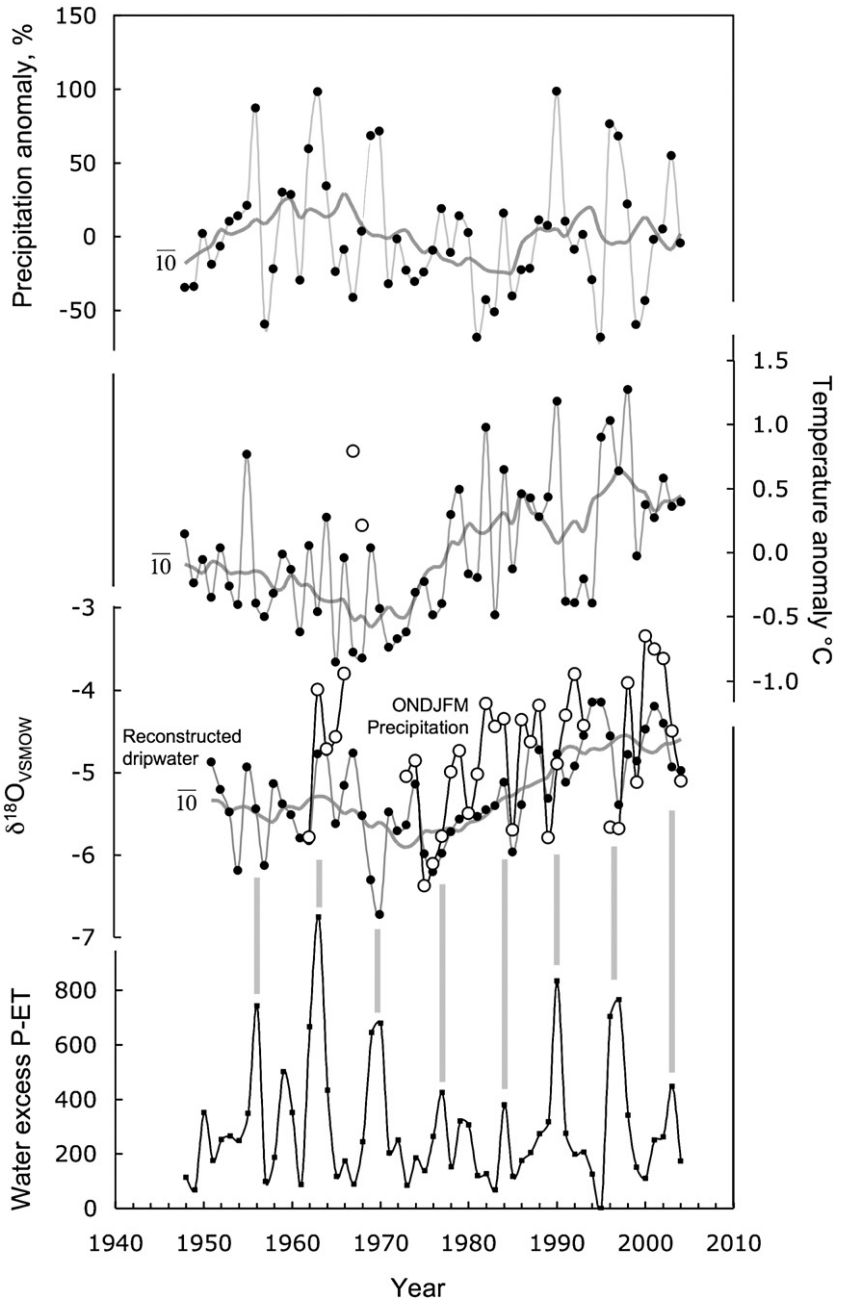

Fig. 9. Correspondence of reconstructed drip water $\delta^{18}O$ with the $\delta^{18}O$ of winter (October–March) precipitation and other climate parameters for the period 1951–2004. From top to bottom: winter precipitation and winter temperature anomalies calculated relative to 1961–2000 average; reconstructed $\delta^{18}O$ of past drip water (see text for explanation); water excess (P-ET) calculated using the Thornthwaite method (Thornthwaite, 1954). The $\delta^{18}O$ of weighted October–March precipitation (IAEA/WMO, 2004) is plotted for comparison as closed circles. Ten year moving averages are shown as grey curves. All data from Table 1 in the Appendix. Meteorological data adapted from Crown copyright data supplied by the Met Office.

et al., 1998; Hua and Barbetti, 2004) in Fig. 8. A response to the atmospheric ^{14}C bomb-pulse is clearly seen in Gib04a and ^{14}C activity increases from 92 percent modern carbon (pMC) in the lowest part of the stalagmite to a peak of over 130 pMC around cycle 34 (assigned as 1970). Activity then decreases to around 106 pMC at the tip of the sample, similar to modern atmospheric ^{14}C activity.

Fig. 8 shows that a ^{14}C age model (see supplementary data in the Appendix for discussion) for Gib04a very closely corresponds to the age of each sample mapped on to the $\delta^{13}C$ time scale. Most samples correspond within one year or less across the 50 year record, except two areas where around 1960 the $\delta^{13}C$ model lags the ^{14}C by 2 years, and at around 1985 where the $\delta^{13}C$ model is ahead of the ^{14}C age by 3 years (Fig. 8). The identification of the ^{14}C bomb-pulse corroborates the timescale based on $\delta^{13}C$ cycles thus the speleothem $\delta^{18}O$ record can be compared with confidence to the precipitation isotope record and other instrumental climate parameters at the inter-annual level.

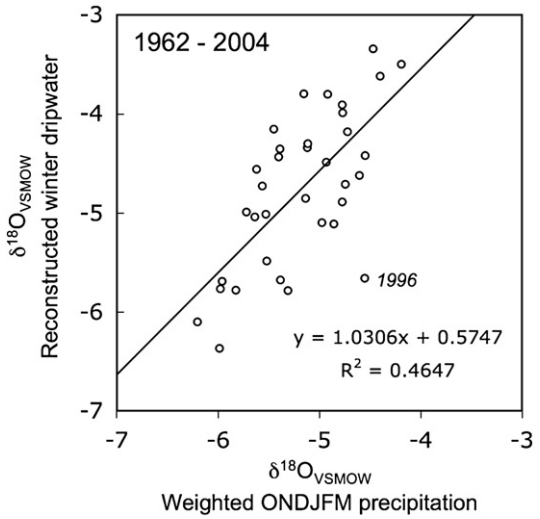

Fig. 10. Correlation of $\delta^{18}O$ of reconstructed winter drip water with $\delta^{18}O$ of weighted October–March precipitation for 1961 to 2004. See text for discussion.

3.7. Comparison of the reconstruction of winter drip water with the Gibraltar precipitation record at inter-annual resolution

The $\delta^{13}C$ minima in Fig. 6 mark the calcite growth in April at a time when the drip water $\delta^{18}O$ value had fallen to their lowest values and become most representative of drip water derived from winter precipitation. For each annual $\delta^{13}C$ minimum the corresponding $\delta^{18}O$ of April calcite has been calculated for each year as the mean of three $\delta^{18}O$ analyses centred on the minimum $\delta^{13}C$ value (Fig. 6). The new $\delta^{18}O$ values are then used to calculate the $\delta^{18}O$ of cave drip water using a calcite water thermometer (O'Neil et al., 1969), and assuming a constant temperature of 18 °C for the cave (see Table 1 in the Appendix).

The inter-annual correspondence of variations in reconstructed winter drip water $\delta^{18}O$ with the $\delta^{18}O$ of October–March precipitation is shown in Fig. 9. Omitting the anomalous precipitation $\delta^{18}O$ values for 1966 and 1967 which are based on just one measurement of a small sample of precipitation (IAEA/WMO, 2004), the two data sets otherwise show a high degree of year-to-year correspondence. The reconstructed drip water curve shows short-term (1–2 years) variations of about 1‰ superimposed on a decreasing trend reaching a minimum around 1970. The isotope curve representing weighted mean October–March precipitation has a very similar structure with excursions that tracks the short-term variations in the drip water curve but at a higher amplitude.

The weighted October–March precipitation $\delta^{18}O$ is plotted against the $\delta^{18}O$ of reconstructed winter drip water plotted in Fig. 10 and shows a significant correlation with $r^2=0.47$ and a slope of ≈ 1. The one obvious outlier in Fig. 10 is at a point where both curves define the edge of a sharp downturn in 1996 (a very wet year) and this sole outlier might be an artefact given an error of ±1 year in the age model. Omitting this point increases r^2 to 0.57. Such good correspondence between the precipitation isotope record and the oxygen isotope signal encoded in speleothem calcite over the longest available precipitation record validates reconstruction of precipitation isotope time series from speleothem calcite in well characterised systems. The main challenge then lies in modelling precipitation isotopes in terms of actual atmospheric processes.

Analysis of the GNIP monthly records reveals neither a strong amount or temperature control on precipitation isotopes (e.g. Hoffmann et al., 1998) but Treble et al. (2005b) have shown that analysis of climate parameters controlling precipitation $\delta^{18}O$ may give very different results at monthly and event levels. The winter precipitation and drip water isotope curves are compared with the winter (October–March) precipitation anomaly, temperature anomaly and water excess in Fig. 9. Many of the excursions to lower $\delta^{18}O$ values seen in the discontinuous precipitation isotope curve coincide almost exactly with very wet years despite the lack of a significant overall amount effect present in the annual or monthly GNIP data (e.g. Hoffmann et al., 1998). The reconstructed drip water curve provides continuous $\delta^{18}O$ data from 1951 and shows that drip water isotope compositions capture the low precipitation $\delta^{18}O$ values that characterise high annual rainfall years (e.g. 1963, 1969/70, 1990 and 1996/7) implying that an 'isotope-amount effect' may be encoded at the inter-annual level. The occurrence of low $\delta^{18}O$ years in the signal structure over longer records may provide indicators of the frequency of wet years or changing moisture sources (Cruz et al., 2005; Treble et al., 2005a). However on a decadal scale the Gibraltar precipitation isotope data shows a secular increase in $\delta^{18}O$ from −5.5‰ in 1975 to −4.5‰ in 2003 which mirrors rising mean winter temperatures over the same period (Fig. 9). There are insufficient data to continue the decadal trend in precipitation isotopes back past 1975 but the higher $\delta^{18}O$ cave seepage water values for this period obtained in this study are also consistent with the higher MAT's that occurred prior to 1975. Unpublished data for Gibraltar precipitation sampled at 12 h event resolution reveals a significant dependence of isotopes on temperature and more work is necessary in order to understand the factors that control precipitation $\delta^{18}O$ in SW Iberia.

The results of this study show that in well characterised cave environments $\delta^{18}O$ time series for speleothem calcite are capable of providing reliable proxies of precipitation and atmospheric processes. Factors favouring this approach require karst aquifers with rapid recharge, minimal attenuation of the winter precipitation $\delta^{18}O$ signal, rapid growth rates and clear cyclical trace element and isotope records which allow winter groundwater to be resolved from biasing effects of surface evaporation.

The winter NAO influences rainfall in Iberia (Xoplaki et al., 2004; Andreo et al., 2004) and –ve NAO conditions result in increased rainfall amount and lower MAT. Reconstruction of past frequency and amplitude of the NAO remains a considerable challenge (Hurrell, 1995) with very few palaeo-NAO data prior to 1700 (Cook, 2003). Seasonally resolved speleothem isotope records encode different climate information over sub-annual, inter-annual and decadal timescales and provide the key to identifying specific processes that control $\delta^{18}O$ variability in speleothem proxies. The results of this work show that long seasonally resolved speleothem records have considerable potential in the reconstruction of precipitation and temperature patterns related to the NAO in this region.

4. Conclusions

An isotope time series measured at 100 μm resolution in a modern speleothem from Gibraltar reveals exceptionally well defined $\delta^{13}C$ and $\delta^{18}O$ cycles that correlate with hydrochemical cycles recorded by trace elements and development of paired light coloured columnar calcite and darker microsparitic calcite fabrics. Monitoring of cave microclimate, cave air pCO_2, hydrology and drip water chemistry provide compelling evidence that the speleothem cycles are annual, and links the speleothem cycles in $\delta^{13}C$, $\delta^{18}O$, trace elements and fabric development to specific seasons in the calendar year. Cave ventilation rather than water excess is believed to be the main factor in controlling fabric development in Gibraltar. The light columnar calcite (LC) fabric develops after pCO_2 sharply rises in November resulting in slower degassing rates, lower calcite supersaturation and falling $\delta^{13}C$. The dark, microporous, microsparitic (DCC) fabric develops after the cave switches to summer mode in April when cave air pCO_2 falls sharply which forces higher degrees of calcite supersaturation and elevated $\delta^{13}C$. Early results of monitoring show that the $\delta^{18}O$ of drip water also evolves following a seasonal pattern where lowest $\delta^{18}O$ drip water representing the previous winters precipitation arrives after the cave switches to summer mode ventilation but before the switch to DCC fabric where kinetic effects become significant. The interplay between the ventilation and hydrological cycles determines whether the climatically important winter precipitation arrives when drip waters are weakly supersaturated and depositing LC or strongly supersaturated and depositing DCC with a higher component of kinetic fractionation.

An age model spanning the period of growth from 1951 to 2004 derived from counting $\delta^{13}C$ cycles has been validated by locating the ^{14}C atmospheric bomb-spike in its correct position. Since $\delta^{13}C$ reaches a minimum value in April at the time when winter precipitation appears in the cave as seepage water the $\delta^{18}O$ characteristics of calcite deposited from drip water representing winter precipitation for each year can therefore be identified. This allows reconstruction of the $\delta^{18}O$ drip water representing winter precipitation for each year from 1951–2004. These data show a high degree of correspondence ($r^2 = 0.47$) with the $\delta^{18}O$ of rainfall falling each year between October and March however the climatic components encoded in the reconstructed precipitation time series are conflicting in terms of amount and temperatures effects and require further analysis.

Speleothem isotope records from sites where a high component of seasonal variation might be expected might yield ambiguous climate signals when sampled at low resolution, either as a result of variations in the proportions of summer and winter growth (Treble et al., 2005a) or where the scale of the sampled domain and seasonal variability are similar (Fairchild et al., 2005). Seasonally resolved time series may not always be a viable proposition but provide rich opportunities for recovering climatically significant information.

Acknowledgements

This work was initiated, with encouragement and assistance from Ted Rose, under NERC grant NER/T/S/2002/00985 and many ideas developed out of discussion among members of the ASCRIBE consortium led by Ian Fairchild. Ongoing work is now supported by NERC grant NE/D005280. We are indebted to J-P Latin and our project partners in the Caves and Cliffs Section, Gibraltar Ornithological and Natural History Society, for skilful management of the cave monitoring program. We thank Clive Finlayson for initial permission to carry out sampling in New St. Michaels Cave and introduction to members of the Caves and Cliffs section of GONHS. Principal Met Officers at the Gibraltar RAF Met Office kindly provided meteorological records, with additional information provided by Dennis Wheeler (University of Sunderland). Tim Atkinson (University College, London) led the 2007 cave survey campaign and provided use of the micromill in the Bloomsbury Environmental Laboratory; the NERC ICPMS facility (University of Kingston) provided laser ablation trace element analyses. Andrea Borsato assisted with reduction of the Sr synchrotron radiation micro-XRF data. U–Th ages were provided by Siobhan McGarry and Dirk Hoffman, University of Bristol. We are grateful to David Alderton (RHUL) for assistance with XRD analysis and SEM imaging. EBSD images were provided by Nicola Cayzer at the SEM Unit, University of Edinburgh. We thank Ian Fairchild, Martin Menzies and anonymous reviewers for constructive comments on early drafts of the manuscript.

Appendix A. Supplementary data

Supplementary data associated with this article can be found, in the online version, at doi:10.1016/j.epsl.2008.01.051.

References

Amundson, R.G., Davidson, E.A., 1990. Carbon dioxide and nitrogenous gases in the soil atmosphere. J. Geochem. Explor. 38, 13–41.

Andreo, B., Liñan, C., Carrasco, F., Jiménez de Cisneros, C., Caballero, F., Mudry, J., 2004. Influence of rainfall quantity on the isotopic composition (^{18}O and ^{2}H) of water in mountainous areas. Application for groundwater research in the Yunquera-Nieves karst aquifers (S Spain). Appl. Geochem. 19, 561–574.

Andreo, B., Jiménez, P., Durán, J.J., Carrasco, F., Vadillo, I., Mangin, A., 2006. Climatic and hydrological variations during the last 117–166 years in the south of the Iberian Peninsula, from spectral and correlation analyses and continuous wavelet analyses. J. Hydrol. 324, 24–39.

Ayalon, A., Bar-Matthews, M., Sass, E., 1998. Rainfall-recharge relationships within a karstic terrain in the Eastern Mediterranean semi-arid region, Israel: $\delta^{18}O$ and δD characteristics. J. Hydrol. 207, 18–31.

Baker, A., Genty, D., 1998. Environmental pressures on conserving cave speleothems: effects of changing surface land use and increased cave tourism. J. Environ. Manag. 53, 165–175.

Bar-Matthews, M., Ayalon, A., Matthews, A., Sass, E., Halicz, L., 1996. Carbon and oxygen isotope study of the active water-carbonate system in a karstic Mediterranean cave: implications for paleoclimate research in semiarid regions. Geochim. Cosmochim. Acta 60, 337–347.

Batiot-Guilhe, C., Seidel, J.-L., Jourde, H., Hébrard, O., Bailly-Comte, V., 2007. Seasonal variations of CO_2 and ^{222}Rn in a Mediterranean sinkhole — spring (Causse d'Aumelas, SE France). Int. J. Speleol. 36, 51–56.

Bourges, F., Mangin, A., d'Hulst, D., 2001. Le gaz carbonique dans la dynamique de l'atmosphère des cavités karstiques: l'exemple de l'Aven d'Orgnac (Ardèche). Earth Planet. Sci. 333, 692–696.

Cook, E.R., 2003. Multi-proxy reconstructions of the North Atlantic Oscillation (NAO) index: a critical review and a new well-verified winter NAO index reconstruction back to AD 1400. In: Hurrell, J.W., Kushnir, Y., Ottersen, G., Visbeck, M. (Eds.), The North Atlantic Oscillation. Climate Significance and Environmental Impact. Geophysical Monograph, vol. 134. AGU, Washington.

Cruz, F.W., Karmann, I., Viana, O., Burns, S.J., Ferrari, J.A., Vuille, M., Sial, A.N., Moreira, M.Z., 2005. Stable isotope study of cave percolation waters in subtropical Brazil: implications for paleoclimate inferences from speleothems. Chem. Geol. 220, 245–262.

Faimon, J., Štelcl, J., Sas, D., 2006. Anthropogenic CO_2-flux into cave atmosphere and its environmental impact: a case study in the Císařská Cave (Moravian Karst, Czech Republic). Sci. Total Environ. 369, 231–245.

Fairchild, I.J., McMillan, E., 2007. Speleothems as indicators of wet and dry periods. Int. J. Speleol. 36, 69–74.

Fairchild, I.J., Borsato, A., Tooth, A.F., Frisia, S., Hawkesworth, C.J., Huang, Y.M., McDermott, F., Spiro, B., 2000. Controls on trace element (Sr–Mg) compositions of carbonate cave waters: implications for speleothem climatic records. Chem. Geol. 166, 255–269.

Fairchild, I.J., Baker, A., Borsato, A., Frisia, S., Hinton, R.W., McDermott, F., Tooth, A.F., 2001. High-resolution, multiple-trace-element variation in speleothems. J. Geol. Soc. 158, 831–841 London.

Fairchild, I.J., Baker, A., Fuller, L., Mattey, D., McDermott, F., Spötl, C., Smith, C.L., 2005. Modification and preservation of environmental signals in speleothems. Earth Sci. Rev. 75, 153–195.

Finch, A.A., Shaw, P.A., Weedon, G.P., Holmgren, K., 2001. Trace element variation in speleothem aragonite: potential for paleoenvironmental reconstruction. Earth Planet. Sci. Lett. 186, 255–267.

Fink, D., Hotchkis, M., Hua, Q., Jacobsen, G., Smith, A.M., Zoppi, U., Child, D., Mifsud, C., van der Gaast, H., Williams, A., Williams, M., 2004. The ANTARES AMS facility at ANSTO. Nucl. Instrum. Methods Phys. Res., B 223–224, 109–115.

Frisia, S., Borsato, A., Fairchild, I.J., McDermott, F., 2000. Calcite fabrics, growth mechanisms, and environment of formation in speleothems from the Italian Alps and southwestern Ireland. J. Sediment. Res. 70, 1183–1196.

Genty, D., Quinif, Y., 1996. Annually laminated sequences in the internal structure of some Belgian stalagmites-importance for paleoclimatology. J. Sediment. Res. 66, 275–288.

Henderson, G.M., 2006. Caving in to new chronologies. Science 313, 620–622.

Hendy, C.M., 1971. The isotopic geochemistry of speleothems — I. The calculation of the effects of different modes of formation on the isotopic composition of speleothems and their applicability as palaeoclimatic indicators. Geochim. Cosmochim. Acta 35, 801–824.

Hoffmann, G., Werner, M., Heimann, M., 1998. Water isotope module of the ECHAM atmospheric general circulation model: a study of timescales from days to several years. J. Geophys. Res.-Atmospheres 103, 16871–16896.

Hoyos, M., Soler, V., Cañavera, J.C., Sánchez-Moral, S., Sanz-Rubio, E., 1998. Microclimatic characterization of a karstic cave: human impact on microenvironmental parameters of a prehistoric rock art cave (Candamo Cave, northern Spain). Environ. Geol. 33, 231–242.

Hua, Q., Barbetti, M., 2004. Review of tropospheric bomb ^{14}C data for carbon cycle modeling and age calibration purposes. Radiocarbon 46, 1273–1298.

Hua, Q., Jacobsen, G.E., U., Z., E.M., L., Williams, A.A., Smith, A.M., McGann, M.J., 2001. Progress in radiocarbon target preparation at the ANTARES AMS centre. Radiocarbon 43, 275–282.

Huang, Y.M., Fairchild, I.J., 2001. Partitioning of Sr^{2+} and Mg^{2+} into calcite under karst-analogue experimental conditions. Geochim. Cosmochim. Acta 65, 47–62.

Hurrell, J.W., 1995. Decadal trends in the North Atlantic Oscillation and its relationships to regional temperature and precipitation. Science 269, 676–679.

IAEA/WMO, 2004. Global network of isotopes in precipitation. The GNIP Database. Accessible at: http://isohis.iaea.org.

Johnson, K.R., Hu, H., Belshaw, N.S., Henderson, G.M., 2006. Seasonal trace-element and stable-isotope variations in a Chinese speleothem: the potential for high-resolution paleomonsoon reconstruction. Earth Planet. Sci. Lett. 244, 394–407.

Jones, P.D., Jonsson, T., Wheeler, D., 1997. Extension to the North Atlantic Oscillation using early instrumental pressure observations from Gibraltar and south-west Iceland,. Int. J. Climatol. 117, 14331450.

Lopez-Bustins, J.-A., Martin-Videa, J., Sanchez-Lorenzo, A. Iberia winter rainfall trends based upon changes in teleconnection and circulation patterns, Global and Planetary Change, Article in Press, Corrected Proof (in press).

Mattey, D., Lowry, D., Fisher, R., 2005. Seasonal and inter-annual climate responses revealed in an ultra-high resolution isotope record in a speleothem from Gibraltar. EOS Trans AGU 86 (52) Fall Meeting Suppl., Abstract PP43A-0609.

Mattey, D., Lowry, D., Fisher, R., Duffet, J., Latin, J.P., Ainsworth, M., Balestrino, J., Durell, R., McCarthy, J., de la Paz, H., 2006. Seasonal changes in the isotopic composition of cave air, water and speleothem calcite in new St. Michaels Cave, Gibraltar: unwanted noise or a tool for decoding speleothem climate records? KarstIV, The Climate Record, Baille Herculane, Romania, May 2006.

McDermott, F., 2004. Palaeo-climate reconstruction from stable isotope variations in speleothems: a review. Quat. Sci. Rev. 23, 901–918.

McDermott, F., Mattey, D.P., Hawkesworth, C., 2001. Centennial-scale holocene climate variability revealed by a high-resolution speleothem delta O-18 record from SW Ireland. Science 294, 1328–1331.

McDermott, F., Schwarcz, H.P., Rowe, P.J., 2006. Isotopes in speleothems. In: Leng, M.J. (Ed.), Isotopes in Palaeoenvironmental Research. Springer, Dordrecht, The Netherlands, pp. 185–226.

McMillan, E., Fairchild, I.J., Frisia, S., Borsato, A., 2005. Calcite-aragonite trace element behaviour in annually layered speleothems: evidence of drought in the Western Mediterranean 1200 years ago. J. Quat. Sci. 20, 423–433.

Mickler, P.J., Banner, J.L., Stern, L., Asmerom, Y., Edwards, R.L., Ito, E., 2004. Stable isotope variations in modern tropical speleothems: evaluating equilibrium vs. kinetic isotope effects. Geochim. Cosmochim. Acta 68, 4381–4393.

Miotke, F.D., 1974. Carbon dioxide and the soil atmosphere, Abhandlungen zur Karst-Und Höhlenkunde, Reihe A, Speläologie. Heft 9.

O'Neil, J.R., Clayton, R.N., Mayeda, T.K., 1969. Oxygen isotope fractionation in divalent metal carbonates. J. Chem. Phys. 51, 5547–5558.

Roberts, M.S., Smart, P., Baker, A., 1988. Annual trace element variations in a Holocene speleothem. Earth Planet. Sci. Lett. 154.

Rodrıguez-Vidal, J., C!aceres, L.M., Finlayson, J.C., Gracia, F.J., Mart!ınez-Aguirre, A., 2004. Neotectonics and shoreline history of the Rock of Gibraltar, southern Iberia. Quat. Sci. Rev. 23, 2017–2029.

Rose, E.P.F., Rosenbaum, M.S., 1991. A Field Guide to the Geology of Gibraltar, The Gibraltar Museum.

Shaw, T.R., 1953a. Old St. Michaels Cave, BSA. Cave Sci. 3, 298–313.

Shaw, T.R., 1953b. New St. Michaels Cave, BSA. Cave Sci. 3, 249–266.
Spotl, C., Fairchild, I.J., Tooth, A.F., 2005. Cave air control on dripwater geochemistry, Obir Caves (Austria): implications for speleothem deposition in dynamically ventilated caves. Geochim. Cosmochim. Acta 69, 2451–2468.
Spötl, C., Mattey, D., 2006. Stable isotope microsampling of speleothems for palaeoenvironmental studies: a comparison of microdrill, micromill and laser ablation techniques. Chem. Geol. 235, 48–58.
Stuiver, M., Reimer, P.J., Braziunas, T.F., 1998. High-precision radiocarbon age calibration for terrestrial and marine samples. Radiocarbon 40, 1127–1151.
Thornthwaite, C.W., 1954. The Measurement of Potential Evapotranspiration: Seabrook. John. P. Mather, New Jersey. 225pp.
Tooth, A.F., Fairchild, I.J., 2003. Soil and karst aquifer hydrological controls on the geochemical evolution of speleothem-forming drip waters, Crag Cave, southwest Ireland. J. Hydrol. 273, 51–68.
Tratman, E.K., 1971. The formation of the Gibraltar Caves. Trans. Cave Res. Group G.B. 13, 135–143.
Treble, P.C., Harrison, T.M., Shelley, J.M.G., McKeegan, K., Grove, M., McCulloch, M.T., 2002. High resolution trace element and oxygen isotope analyses of a modern speleothem. Geochim. Cosmochim. Acta 66, A784–A784.
Treble, P.C., Chappell, J., Gagan, M.K., McKeegan, K.D., Harrison, T.M., 2005a. In situ measurement of seasonal delta O-18 variations and analysis of isotopic trends in a modem speleothem from southwest Australia. Earth Planet. Sci. Lett. 233, 17–32.
Treble, P., Budd, W.F., Hope, P.K., Rustomji, P.K., 2005b. Synoptic-scale climate patterns associated with rainfall delta O-18 in southern Australia. J. Hydrol. 302, 270–282.
Wasylenki, L.E., Dove, P.M., Wilson, D.S., De Yoreo, J.J., 2005. Nanoscale effects of strontium on calcite growth: an in situ AFM study in the absence of vital effects. Geochim. Cosmochim. Acta 69, 3017–3027.
Wheeler, D., 2006. The Gibraltar climatic record: part 1 — the history of weather observations. Weather 61, 36–39 (published by the Royal Meterological Society).
Wright, E.P., Rose, E.P.F., Perez, M., 1994. Hydrogeological studies of the Rock of Gibraltar. Q. J. Eng. Geol. 27, S15–S29.
Xoplaki, E., González-Rouco, J.F., Luterbacher, J., Wanner, H., 2004. Wet season Mediterranean precipitation variability: influence of large-scale dynamics and trends. Clim. Dyn. 23, 63–78.
Yonge, C., Ford, D.C., Gray, J., Schwarcz, H.P., 1985. Stable isotope studies of cave seepage water. Chem. Geol. 58, 97–105.
Yuan, D., Cheng, H., Edwards, R.L., Dyoski, C.A., Kelly, M.J., Zhang, M., Qing, J., Lin, Y., Wang, Y., Wu, J., Dorale, J., An, Z., Cai, Y., 2004. Timing, duration and transitions of the last interglacial Asian monsoon. Science 304, 575–578.